REPORT DOCUMENTATION PAGE

Form Approved
OMB No. 0704-0188

1. REPORT DATE *(DD-MM-YYYY)*	**2. REPORT TYPE**	**3. DATES COVERED** *(From - To)*
5/10/2011	Final Report	7/1/2009-2/28/2011

4. TITLE AND SUBTITLE

Supersonic Inlet Flow Control Using Localized Arc Filament Plasma Actuators

5a. CONTRACT NUMBER

5b. GRANT NUMBER
FA9550-09-1-0644

5c. PROGRAM ELEMENT NUMBER

6. AUTHOR(S)

Samimy, Mo, Webb, Nathan and Clifford, Christopher
Gas Dynamics and Turbulence Laboratory
Aeronautical and Astronautical Research Laboratory
Department of Mechanical and Aerospace Engineering
The Ohio State University
2300 West Case Road; Columbus, Ohio 43235

5d. PROJECT NUMBER

5e. TASK NUMBER

5f. WORK UNIT NUMBER

7. PERFORMING ORGANIZATION NAME(S) AND ADDRESS(ES)

The Ohio State University
Aeronautical and Astronautical Research Laboratory
Department of Mechanical and Aerospace Engineering
2300 West Case Road; Columbus, Ohio 43235

8. PERFORMING ORGANIZATION REPORT NUMBER

AFOSR-OSU-GDTL1011

9. SPONSORING / MONITORING AGENCY NAME(S) AND ADDRESS(ES)

AFOSR
875 N Randolph St
Arlington, VA 22203

10. SPONSOR/MONITOR'S ACRONYM(S)

11. SPONSOR/MONITOR'S REPORT NUMBER(S)
AFRL-OSR-VA-TR-2012-0738

12. DISTRIBUTION / AVAILABILITY STATEMENT

Unlimited.

13. SUPPLEMENTARY NOTES

14. ABSTRACT

Shock Wave/Boundary Layer Interactions (SWBLIs) occur in many applications of interest to the U.S. Air Force and could pose significant problems depending on the specific application. This study has undertaken to investigate the use of Localized Arc Filament Plasma Actuators (LAFPAs) to control SWBLIs with the objective of mitigating/eliminating separation. Initial experiments were carried out in a small Mach 2 tunnel with compression ramp. The results showed that the LAFPAs are capable of significantly energizing the flow within the interaction region when located upstream of the reflected shock. The maximum control authority was found to be exercised when the LAFPAs were operated at a Strouhal number of 0.03. This frequency is similar to that at which the reflected shock oscillates in unforced SWBLIs. Therefore, LAFPAs are believed to manipulate the natural instability associated with the reflected shock oscillation. The success of the preliminary experiments motivated the design of a new, larger, more flexible facility that utilize a Variable Angle Wedge to generate the impinging shock wave for SWBLI. This facility is capable of easily generating a wide range of SWBLI strengths. The research is currently on-going.

15. SUBJECT TERMS

16. SECURITY CLASSIFICATION OF:			**17. LIMITATION OF ABSTRACT**	**18. NUMBER OF PAGES**	**19a. NAME OF RESPONSIBLE PERSON**
a. REPORT	**b. ABSTRACT**	**c. THIS PAGE**			**19b. TELEPHONE NUMBER** *(include area code)*

Supersonic Inlet Flow Control Using Localized Arc Filament Plasma Actuators

Mo Samimy, Nathan Webb, and Christopher Clifford
Gas Dynamics and Turbulence Laboratory
Aeronautical and Astronautical Research Laboratory
Department of Mechanical and Aerospace Engineering
The Ohio State University
2300 West Case Road
Columbus, Ohio 43235
samimy.1@osu.edu; (614) 292-5012

Final Report for Air Force Office of Scientific Research (FA9550-09-1-0644)

For Period of 7/1/2009 to 2/28/2011

Abstract

Shock Wave/Boundary Layer Interactions (SWBLIs) occur in many applications of interest to the U.S. Air Force and could pose significant problems depending on the specific application. In supersonic mixed compression inlets, they could initiate unstart by inducing boundary layer separation. This study has undertaken to investigate the use of Localized Arc Filament Plasma Actuators (LAFPAs) to control SWBLIs with the objective of mitigating/eliminating separation. Initial experiments were carried out in a small *Mach* 1.9 tunnel with compression ramp. The results showed that the LAFPAs are capable of significantly energizing the flow within the interaction region when located upstream of the reflected shock. The maximum control authority was found to be exercised when the LAFPAs were operated at a Strouhal number of 0.03 (~ 1 kHz). This frequency is similar to that at which the reflected shock oscillates in unforced SWBLIs. Therefore, LAFPAs are believed to manipulate the natural instability associated with the reflected shock oscillation. The success of the preliminary experiments motivated the design of a new, larger, more flexible facility that utilize a Variable Angle Wedge (VAW) (rather than a compression ramp) to generate the impinging shock wave for SWBLI. This facility is capable of easily generating a wide range of SWBLI strengths, but was found to be a poor environment for testing the LAFPAs control authority due to its inability to modify the LAFPA location. The necessary modifications to add this capability to the facility have been performed. This research is currently continuing with the focus on investigating the actuation authority and mechanism at various SWBLI strengths as well as on the optimization of the control authority.

Acknowledgments

The support of this research by the Air Force Office of Scientific Research with Dr. Jon Schmisseur and by the Air Vehicle Directorate of the Air Force Research Laboratory is greatly appreciated.

Table of Contents

1 Introduction

FLOW separation, the reversal of fluid motion, can be the source of many problems in aerodynamic applications. When separation occurs, the flow becomes unsteady, significantly altering the performance of the system in question. Flow separation generally occurs when the dynamic pressure near a surface is insufficient to negotiate an imposed adverse pressure gradient, as in across a shock wave. For this reason the shock wave/boundary layer Interaction (SWBLI) has been extensively studied for over 60 years.[1]

A SWBLI occurs when a shock forms on a surface with a boundary layer, or when a shock impinges on such a surface. These configurations both result in the shock imposing an adverse pressure gradient. If the interaction/shock is strong enough the low momentum fluid in the boundary layer is unable to negotiate the pressure gradient, and the flow separates. A schematic of an impinging oblique SWBLI with separation is shown in Figure 1. SWBLIs are ubiquitous in supersonic and hypersonic flows. They are especially prevalent in supersonic mixed-compression inlets, in which, flow separation reduces the effective area of the inlet resulting in a low mass flow delivered to the engine. Additionally unsteadiness generated by the separation may cause large fluctuating pressure loads that could damage engine components. In severe cases, the unsteadiness may destabilize the terminal normal shock resulting in unstart.

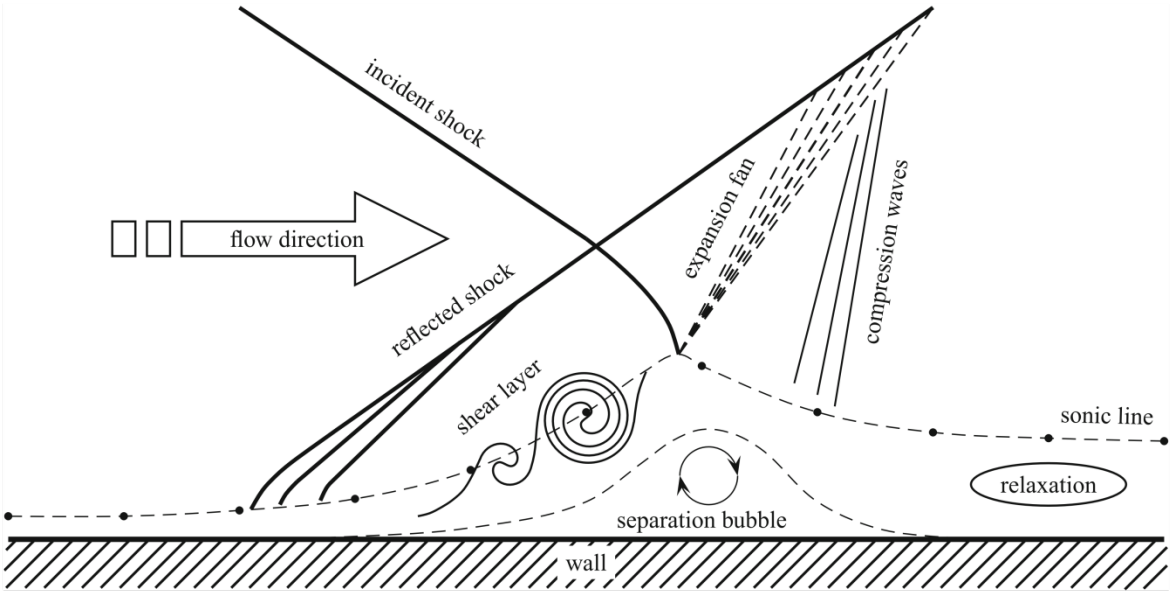

Figure 1: Schematic of a Typical Oblique SWBLI.[2]

The consequences of separation make control of the flow to prevent separation a necessity for high-speed propulsion. Boundary layer bleed is currently the method of choice for separation prevention in supersonic inlets. The control is introduced by removing ("bleeding") low momentum fluid in the boundary layer from the inlet upstream of the SWBLI. This ensures that any flow susceptible to separation by the shock does not reach the SWBLI. This method, although effective, is inherently detrimental to the performance of the engine. Energy produced by the engine must be used to bleed the flow. Additionally both the reduced mass flow (necessitating a larger inlet nacelle) and the bleed and dumping systems increase the weight and drag of the inlet, further reducing the engine performance.[3]

The inefficiency of boundary layer bleed as a separation prevention technique has spurred research into alternate SWBLI control methods. Many examples of passive control methods exist. Vortex generators submerged in the boundary layer are currently being evaluated as an alternate control method by many research groups.[4,5] Three-dimensional bumps have been investigated by Ogawa and Babinsky[6] as a means of modifying the shock structure to reduce the total pressure losses and the likelihood of separation. Gefroh et al.[7] installed a plenum chamber below the SWBLI with flaps to recirculate fluid within the chamber. The goal was to inject momentum into the boundary layer upstream of the interaction, resulting in a healthier boundary layer that is more resistant to separation.

Although passive control techniques have the advantage of not consuming power, a careful examination of each of the above techniques will reveal a common weakness: each is highly sensitive to the location of the geometric modifications. The consequence of this sensitivity is that passive control techniques do not generally perform well under off-design conditions. Although active techniques require power to operate, they often provide much greater flexibility. Such techniques offer dynamic control and can be turned off when not needed to reduce power consumption.

1.1 SWBLI Unsteady Behavior

The goal of an active control technique is to implement the desired alteration in a flow with as little input power as possible. This is generally achieved by exploiting natural instabilities in the flow to amplify the effects of the control input. In this manner, small, low power perturbations can be used to introduce significant changes to the overall flow. In order to take full advantage of this method, a clear understanding of the physics of the flow is necessary. The general steady structure of the SWBLI is well known[1]; however, the unsteadiness characteristics of the interaction often leading to peak pressure and heat loading are not currently well understood. This understanding is critical to allow for optimum application of active control techniques for separation prevention.

Currently one of the most baffling aspects of the SWBLI is the unsteady motion of the foot of the reflected shock. Intuitively, the shock foot would be expected to undulate due to turbulence in the upstream boundary layer. If so, this oscillation would be at a relatively high frequency due to the high speed of the flow and high convective velocity of the upstream structures. However, the shock foot has been observed to oscillate at a low frequency, approximately two orders of magnitude below the expected frequency, in a largely two-dimensional manner.[2,8] The shock is, as expected, also observed to oscillate in a three-dimensional undulating manner at frequencies native to the upstream boundary layer. This would seem to indicate that another mechanism is at work to generate the large-scale, low-frequency

oscillations. A determination of this mechanism could provide significant insights into a method of exploiting the natural instabilities of the SWBLI to introduce control efficiently.

There are currently two schools of thought regarding the source of the low-frequency oscillations. The first is that the oscillations stem from influences upstream of the interaction, originally proposed by Plotkin.[9] Beresh et al.[10] and Ganapathisubramani et al.[11] have observed "superstructures" in the upstream boundary layer. The term "superstructures" refers to regions of high- and low-speed flow that have a large streamwise extent (up to 70δ). Their presence has also been observed by Humble et al.[12], although they were not able to measure lengths of 70δ. The second theory is that the oscillations stem from influences downstream of the interaction. Piponniau et al.[13] proposed that the shear layer between the separated flow in the interaction region and the attached flow above it is the source of unsteadiness, and Agostini et al.[14] provided more evidence for this explanation. Pirozzoli and Grasso[15] believe an acoustic feedback loop within the subsonic region of the interaction may be the source of unsteadiness. Recent work has shown that a variety of mechanisms may be responsible for the various unsteadiness frequencies observed.[14]

1.2 Current Active Control Research

Investigation into active control techniques for separation prevention in SWBLIs is currently being conducted by various research groups. Kalra et al.[16] are using magnetically accelerated surface plasma. Narayanaswamy et al.[17] are operating plasma driven cavity jets upstream of the reflected shock foot and observing the effects on the SWBLI. Leonov et al.[18] are also using a high-power arc discharge to modify the interaction and mitigate the effects of the shock-induced adverse pressure gradient.

Localized Arc Filament Plasma Actuators (LAFPAs) have been developed at the Gas Dynamics and Turbulence Laboratory (GDTL) at The Ohio State University. Originally these actuators were developed to control high-speed, high-Reynolds number jets for mixing enhancement and noise mitigation.[19-21] LAFPAs assert their control in the jet by using natural instabilities in the flow to amplify the generated perturbations. This report details the investigation of the LAFPA's control authority in a SWBLI. The goal of this research is to examine systematically the effects of the LAFPAs on the SWBLI and to explore the physical mechanism by which the actuators implement their control authority.

This research was carried out in two parts demarcated by which of two test facilities the experiments were used. The first facility is identified by its use of a compression ramp to generate the impinging shock. The experiments performed in this facility were preliminary and exploratory in nature due to the limits of the facility. After verifying that the LAFPAs were able to control a SWBLI, a larger, more flexible wind tunnel was designed and constructed. The new wind tunnel uses a much more versatile variable-angle wedge (VAW) to generate the impinging shock. This facility is being used to conduct much more in-depth and systematic experiments to characterize the actuator's control authority, and to research the physical mechanism by which they assert control over the SWBLI.

2 Experimental Arrangement

2.1 Compression Ramp Facility

The compression ramp facility is located at the Gas Dynamics and Turbulence Laboratory (GDTL) at The Ohio State University. Figure 2 shows a photograph of the compression ramp test section with a side window removed. The blow-down type tunnel uses compressed, dried air to run continuously over a wide range of speeds from subsonic to supersonic by changing the installed nozzle. The current nozzles for Mach 1.5, 2.0, and 2.5 have been designed using the method of characteristics. The focus of the current work is on a flow with a design Mach number of 2.0 and a measured Mach number of 1.9. Before entering the nozzle, flow is directed through a stagnation chamber and the free-stream turbulence is reduced with various screens. The test section is rectangular with dimensions of 76.2 mm wide and 38.10 mm tall. The impinging shock is generated by a 10° ramp located on the top wall of the tunnel (Figure 2). The floor of the test section houses the actuators and has been designed in a modular fashion to allow for easy removal and replacement (Figure 2). The test section is bounded by optical grade fused silica windows on the top and sides. The top and side windows can be replaced with aluminum inserts that have a series of static pressure ports that are used to measure the static pressure distribution. Once the air leaves the test section, it enters a smooth contoured diverging nozzle before it exhausts to the ambient atmosphere.

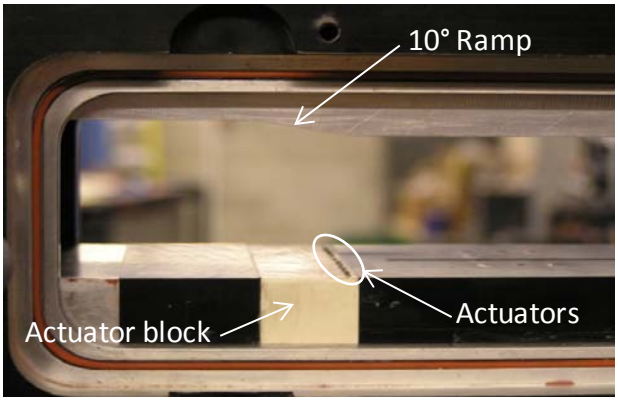

Figure 2: Photograph of the Compression Ramp Facility Section.

2.2 Variable Angle Wedge Facility

After performing experiments in the compression ramp facility, it was concluded that a larger, more flexible wind tunnel was needed to explore the capabilities of the LAFPAs efficiently and effectively. The result of this redesign and the subsequent debugging can be found in Clifford.[22] The final iteration of the design is detailed in this section.

The most recent iteration of the variable-angle wedge facility is a Mach 2.33 blowdown style supersonic wind tunnel located at the GDTL. The test section of the tunnel is 76.2 mm wide by 72.9 mm tall. A variable-angle wedge that acts as a shock generator is located in the freestream flow near the

tunnel ceiling. Figure 3 shows a virtual rendering of the facility. In the current work, the wedge spans only 66.2 mm to allow sidewall boundary layers to pass without deflection and can be varied continuously from 0° to 12.5°.

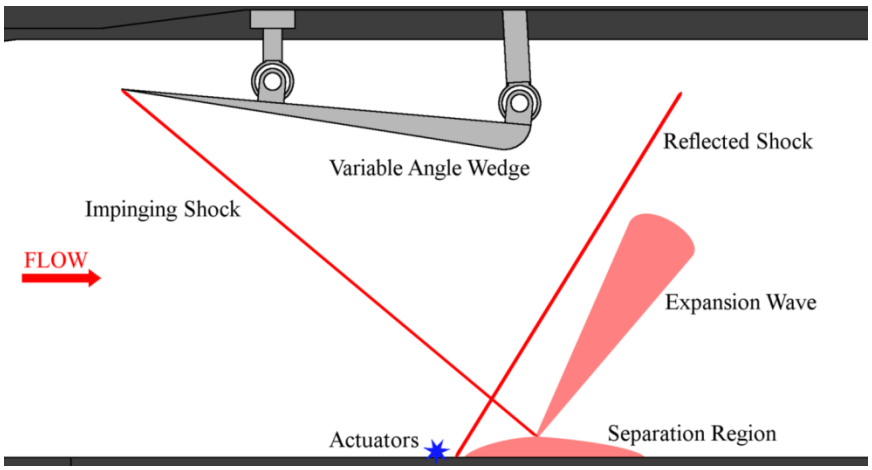

Figure 3: VAW facility schematic.

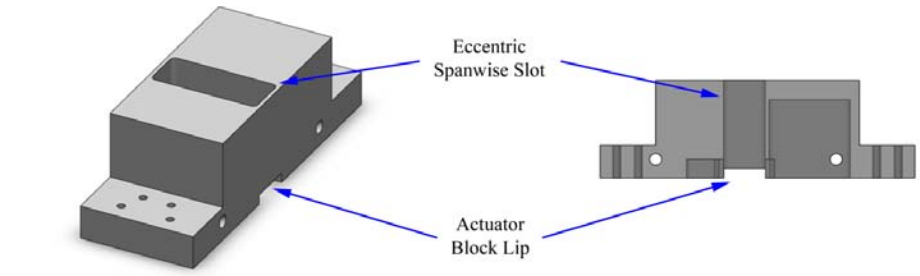

a)

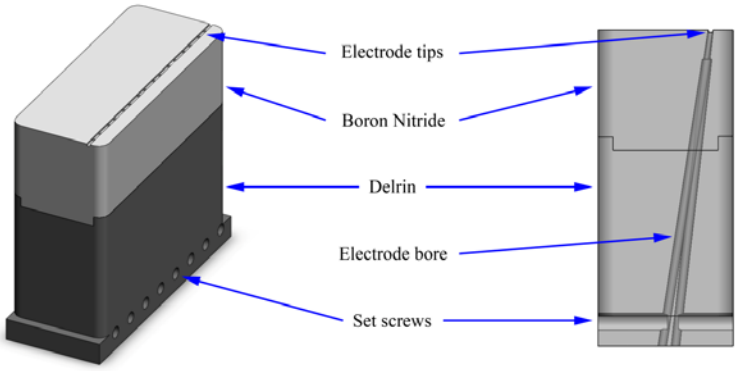

b)

Figure 4: Actuator Block Floor Assembly; a) Floor Cartridge, b) Actuator Block.

A modular test section floor allows for convenient modification of the shock impingement surface for measurement or control purposes (see Figure 4). Two test section floors are used: a floor with an array of pressure transducers and a floor that houses the plasma actuators. Visual access to the test section is provided by fused-silica quartz windows on either side of the test section. The window is 72.9 mm high and extends 250 mm (in the streamwise direction.

The high-pressure storage tanks used in this blow-down facility are sufficient to run the facility continuously. The combined flow rate of the three compressors used to fill the tanks is larger than the wind-tunnel flow rate. However, other constraints effectively limit the useful run-time of the facility. PIV is one of the diagnostics tool used to observe the flow. Olive oil particles are used to seed the flow for these measurements. The streaking of oil particles on the windows could slowly affect the PIV imaging and limit run-time. Thus, with the current setup, accurate data can only be collected for just over a minute. Additionally the flow temperature was calculated (via one-dimensional isentropic flow relations) to be approximately 130 K. Thermal expansion causes the different materials (e.g. aluminum for the floor and boron nitride for the actuator block) used to construct the facility to contract differently, limiting the run-time for non-PIV measurements to approximately 5 minutes. A longer run could cause the windows to crack under stress due to the thermal compression of the rest of the tunnel.

2.3 Plasma Actuators

The spatial arrangement of the LAFPAs in both the compression ramp and VAW facilities is identical. An array of eight LAFPAs is arranged across the span of the tunnel (a photograph of LAFPAs while they are operating in the VAW facility is shown in Figure 5). Each plasma actuator is a pair of 1 mm diameter tungsten electrodes with 3.5 mm center-to-center spacing. The 3 in. wide test section of both facilities therefore requires a spacing of 8.5 mm between the centerline of adjacent actuators (electrode pairs). Application of a sufficiently high voltage causes breakdown of the air between the two electrodes of a LAFPA to occur, initiating an arc filament, which generates rapid localized heating. A 0.5 mm deep groove in the test section floor houses the exposed electrode tips and shields the plasma from the flow. This enables the arc to achieve a quasi-steady operation. It has been shown recently that the groove does not play a significant role in the control process.[23] The actuators have a wide bandwidth from 0 to 200 kHz and each can be operated independently. In the present study, the actuators are mostly fired simultaneously with each other. In one noted instance however, they are fired half a period out of phase with each adjacent actuator. Thus, every other actuator fires simultaneously half a period after the other four fire. For more information on the characterization of plasma actuators, see Utkin et al.[21], and for actuation mechanism, see Samimy et al.[24]. The implementation of the actuators is similar for both facilities.

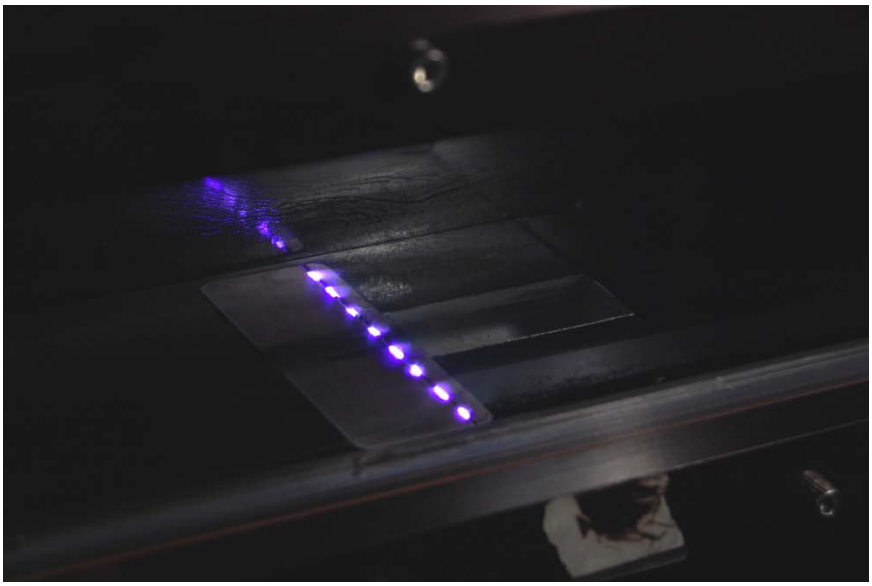

Figure 5: A Photograph of Eight Localized Arc Filament Plasma Actuators in the Tunnel Floor While Active.

2.4 Measurement Diagnostics

Both the compression ramp and the VAW facility had good optical access to the test section; therefore, most of the measurement techniques are optically based. Schlieren, PIV (stereo-cross-stream and 2D-streamwise), and surface oil flow visualization (SOFV) were the primary diagnostics. Time resolved pressure measurements were also made in the VAW facility.

2.4.1 Compression Ramp Measurement Diagnostics

Schlieren imaging was used to verify the quality of the flow in the facility and to ensure that the size and shape of the SWBLI region agree with existing literature. The configuration of the mirrors, light source, camera and the required optics for the schlieren setup are shown in Figure 6. The light source for the system is a Palflash 501 High Intensity Illumination Flash. The light is collimated by a concave parabolic mirror and directed into the test section. After passing through the test section, the light reflects from another parabolic mirror to a plane mirror that directs the light into the camera as shown in Figure 6. A horizontal knife-edge is placed near the downstream focal point of the light to reveal the density gradient in the vertical direction. A similar Z-type schlieren setup was used when performing schlieren in the VAW facility.

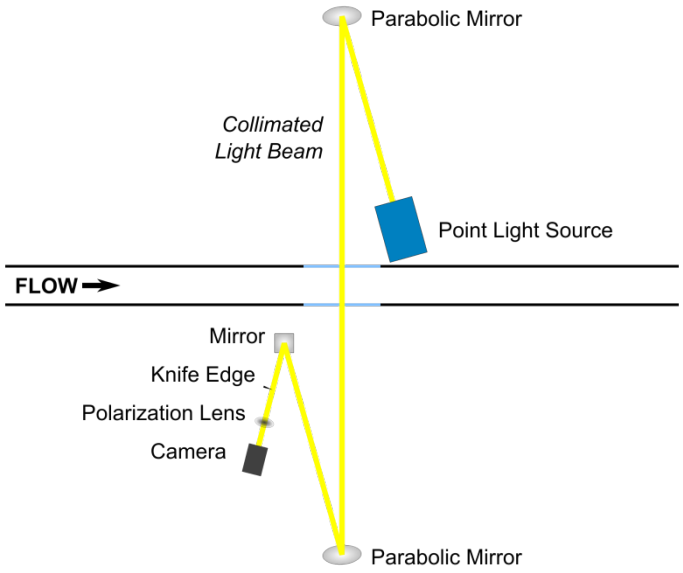

Figure 6: Schematic of Schlieren Imaging Experimental Setup.

Stereoscopic particle image velocimetry (PIV) data is acquired and processed at several cross-stream planes using a LaVision system (DaVis 7.1). The light source is a Spectra Physics PIV 400 Nd:YAG laser. The beam is passed through cylindrical and spherical convex lenses to form it into a thin sheet. The stereo setup consists of two 2k×2k CCD cameras (LaVision ImagerPro) with Tamron 90 mm lenses on either side of the tunnel downstream of the test section. A schematic of the PIV setup can be seen in Figure 7a. The cameras are fitted with a narrow bandpass optical filter to eliminate image contamination due to ambient light and the arc filaments. The flow is seeded with olive oil particles by a TSI six-jet atomizer in the tunnel stagnation chamber. Velocity calculations are done using decreasing window size multipass processing. A 64×64 pixel window with 50% overlap is used for the initial pass while a 32×32 pixel window with 75% overlap is used in the second and third passes. The resulting spatial resolution of the velocity fields is approximately 0.43 mm. Spurious vectors are removed by post-processing using an allowable vector range, correlation peak ratio criteria and a median filter. Eliminated vectors are

reinserted based on a median filter and interpolation scheme. A final 3×3 smoothing filter is applied to the velocity fields.

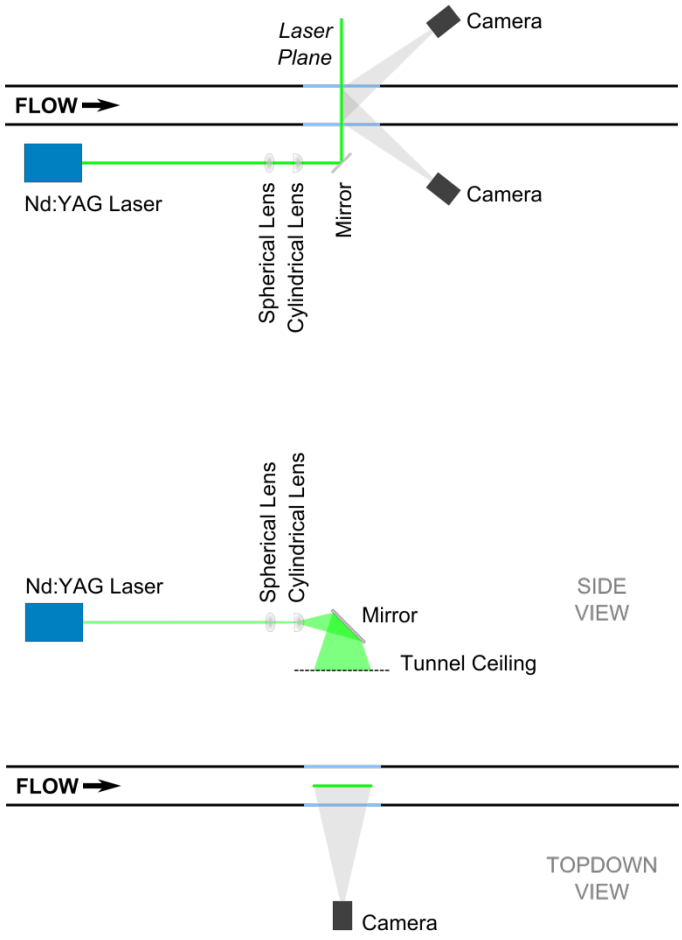

Figure 7: Schematic of PIV Experimental Arrangement;
a) Spanwise Viewing Plane, b) Streamwise Viewing Plane.

2.4.2 Variable Angle Wedge Measurement Diagnostics

Schlieren imaging and surface oil flow visualization provided a qualitative assessment of the flow conditions. Surface oil flow visualization utilizes boundary layer shear forces to form streaklines in oil spread on the tunnel floor. The streaklines then provide insight into the separation region, such as length and three-dimensional characteristics.

PIV is the primary investigative technique. The PIV used for this study measures two components of velocity on a streamwise-vertical plane illuminated by a laser sheet. The resultant velocity maps are used to evaluate boundary layer development, interaction, and recovery in both forced and unforced cases. See Figure 7b for a schematic of this configuration of the PIV system.

The separation region is further characterized using unsteady static pressure measurements. A streamwise array of Kulite pressure transducers placed along the centerline of the tunnel floor provided time-resolved pressure measurements. An auxiliary set of pressure transducers were located halfway between the centerline and the wall to observe potential three-dimensionality. A diagram of the transducer arrays is shown in Figure 8. The pressure transducers were connected to an in-house data acquisition system. Due to spatial averaging effects and the roll-off frequency of the transducers, the signals are low-pass filtered at 25 kHz to prevent aliasing. The filtered signal was collected using a National Instruments BNC 2110 DAQ board. A LabVIEW program provided the graphical interface during experimentation. The signals were then post-processed within MATLAB. As shown in Figure 8, the "centerline" transducers are not on the true tunnel centerline, but are staggered on either side of it. Section 3.2.1.3 will detail the investigation of the two-dimensionality of the interaction and the justification of this arrangement.

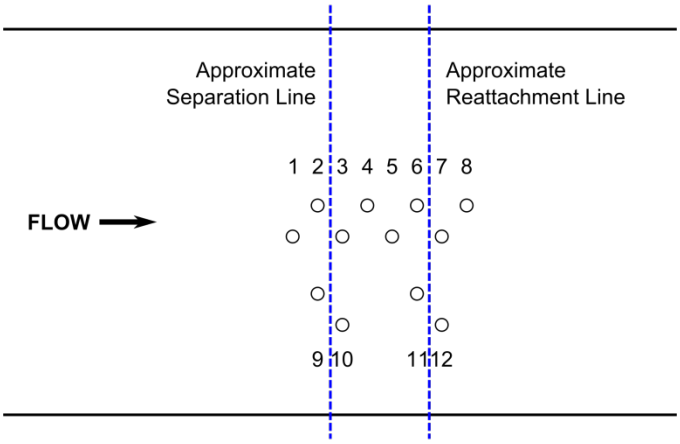

Figure 8: Pressure Transducer Array Distribution.

3 Results and Discussion

3.1 Compression Ramp Results

3.1.1 Baseline Results

Schlieren images were used to verify the quality of the flow. After ensuring that the flow had no unexpected shock/expansion waves, the baseline flow was characterized by taking stereoscopic PIV measurements at the eight different spanwise planes shown in Figure 9. The streamwise reference location (X^*=0) was chosen to be the theoretical inviscid impingement point of the primary shock, as shown in Figure 9.

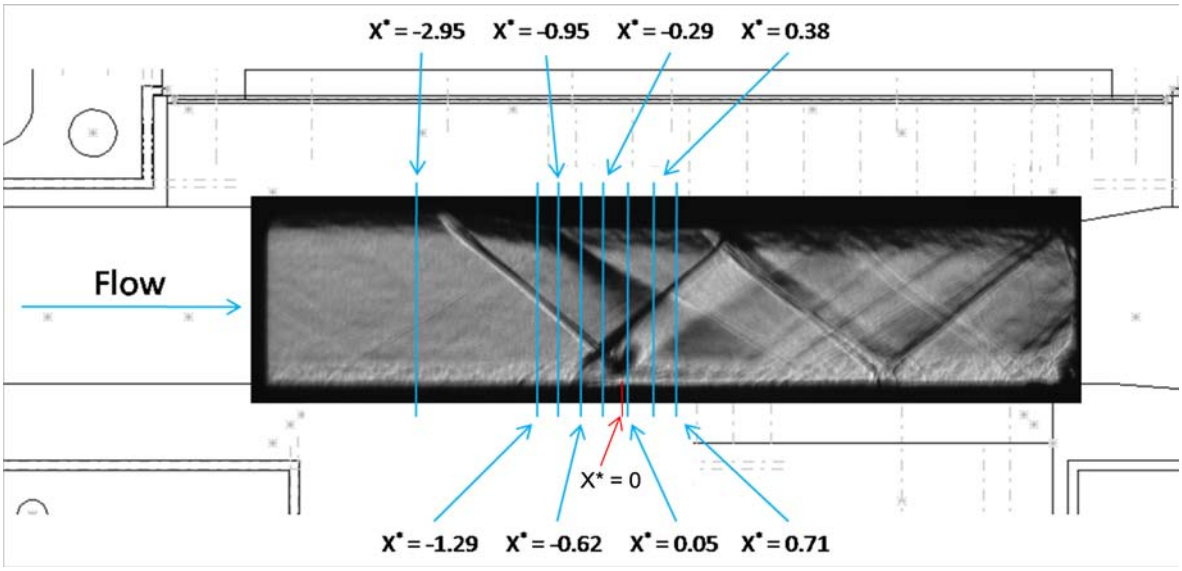

Figure 9: Schlieren Image Showing PIV Measurement Planes for the Baseline Flow Characterization.

The u-component velocity maps from PIV are shown in Figure 10. Each velocity map is an average of 700 images. The evolution of the flow as the measurement plane moves through the oblique shock and the expansion fan can be clearly seen. At the most upstream location, no shock wave is present (Figure 10a). As the measurement plane moves downstream there is a clear decrease in the streamwise velocity component in the upper part of the velocity map indicative of flow passing through the oblique shock (Figure 10b,c) This is followed by a partial recovery in freestream velocity due to the passage of the expansion fan (Figure 10d-h). The effect of the expansion fan can be first noticed in the X^* = -0.62 plane (Figure 10), near the top of the flow, and is estimated to finally reach the floor boundary layer at about X^* = 0.38. The height of the tunnel (38.1 mm) limits the streamwise extent of the 'clean' flow that can be investigated. For the next step of the work, a tunnel with a larger height will be used.

As expected, an increase in boundary layer height due to the shock induced separation can be observed and appears to reach a maximum between the X^* = -0.62 and X^* = 0.05 planes (Figure 10d-f). A subsequent decrease in the height of the boundary layer is also seen in the velocity maps starting between X^* = 0.05 and X^* = 0.38 (Figure 10f,g) and continuing to beyond the farthest downstream PIV measurement plane. However, the boundary layer never completely recovers to its original state due to the presence of repeated reflected shock and expansion waves.

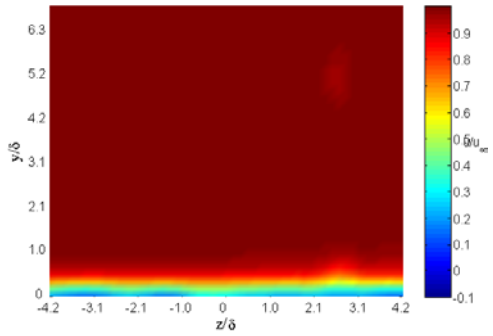

a) X* = -2.95

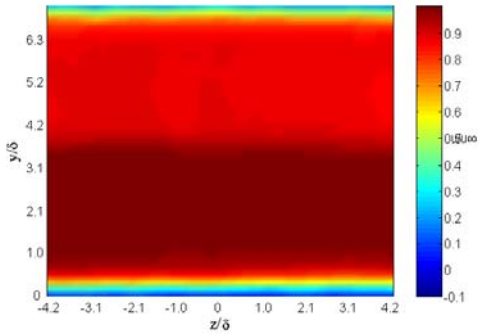

b) X* = -1.29

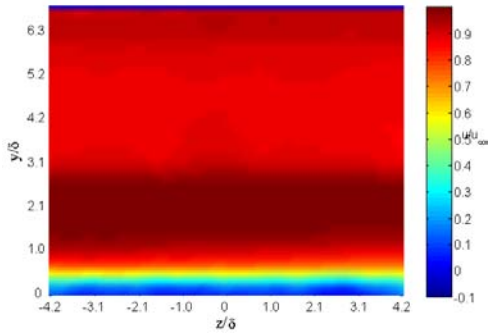

c) X* = -0.95

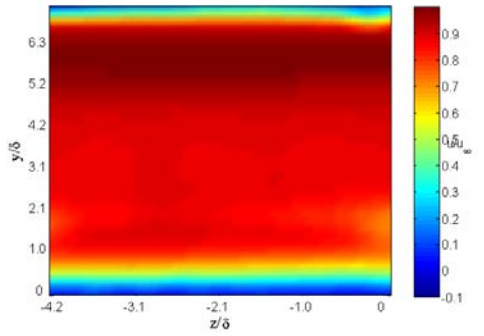

d) X* = -.062

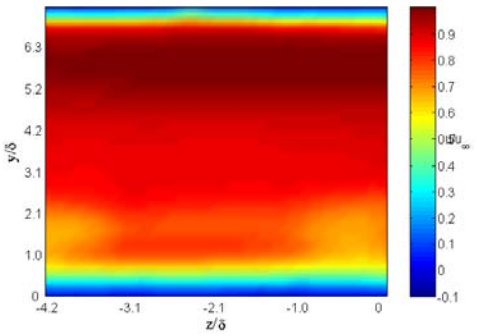

e) X* = -0.29

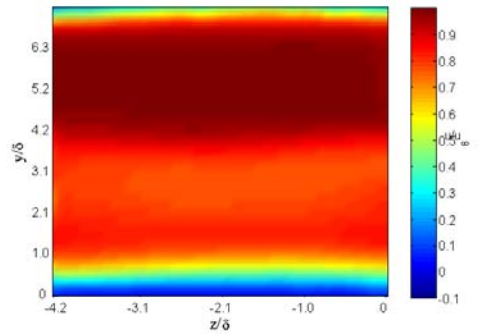

f) X* = 0.05

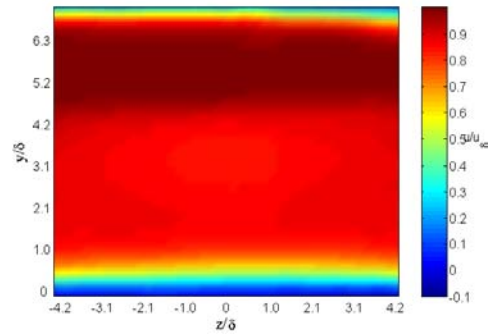

g) X* = 0.38

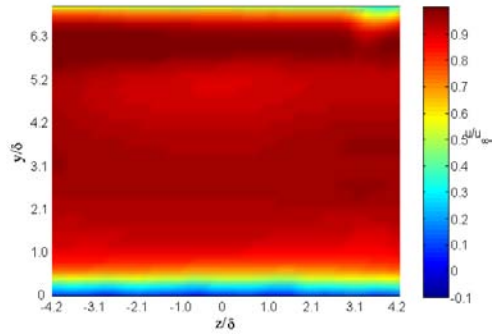

h) X* = 0.71

Figure 10: Streamwise Velocity Maps for the Baseline Case at Eight Streamwise Locations.

3.1.2 Controlled Cases

This preliminary investigation was intended to demonstrate the control ability of LAFPAs for SWBLI while also exploring some of the different parameters such as the forcing Strouhal number and the phase difference between actuators at which the control ability is maximized. Accordingly, it was decided to begin the investigation by selecting a small range of Strouhal numbers over which the control ability could be significant and then to vary the phase difference between actuators.

The initial test plane for these measurements was chosen within the SWBLI region ($X^* = -0.29$), in order to collect data on the effect of the actuators inside this critical region of the flow field. Several sets of measurements were taken at this plane to investigate the effect of the frequency, phase delay between actuators and the location of the actuators and its ability to affect the flow. PIV measurements were taken for Strouhal numbers of 0.03, 0.06, 0.13, 0.25, 0.37 and 0.5, for both forcing methods at actuator locations of $X_a^* = -1.25$ and $X_a^* = -0.83$. The duty cycle was held constant at 30% throughout this study. Due to time and data storage constraints, only 250 images were collected for each test case. Future work will examine the effect of varying duty cycle as well.

Figure 11 shows the streamwise velocity profile for the baseline and various forcing cases when the actuators are located at $X_a^* = -1.25$. This profile is on the centerline of an actuator and has been observed to represent the typical behavior of the flow across the tunnel span. To date, this actuator location has been the most successful for reducing the effect of the SWBLI in the current set up. In this case, the actuators are located slightly upstream of the upstream leg of the λ-shock. In the boundary layer, the normalized velocity shows a significant increase from ~0.08 to ~0.35 near the wall between the baseline and $St_F = 0.03$ (f = 1 kHz) cases. Note that the velocity should be zero at the wall, but the PIV measurement cannot be extended to the wall due to PIV resolution as well as light reflection from the surface. It is clear that the effect of actuation varies significantly with forcing frequency. The case for $St_F = 0.06$ gives a similar amount of control as the $St_F = 0.03$, but as the forcing Strouhal number is further increased, there is a noticeable reduction in the control ability of the actuators. In fact, for $St_F = 0.37$, the effect of actuation has become extremely small and for the case of $St_F = 0.5$ the velocity profile is almost identical to that of the baseline flow. For this specific case, the actuators at $X_a^* = -1.25$, and the measurement plane at $X^* = -0.29$, forcing at $St_F = 0.03$ gives the best result. This suggests that the dominant frequency of the leading leg of the λ-shock structure, as defined in the literature for a similar configuration[25] may play an important role in the LAFPA's ability to control the SWBLI.

Figure 12 shows the u-component of the velocity for three of the cases shown in Figure 11. It is clear from the velocity maps that the forcing frequency has a significant effect on the velocity distribution over the span covered by the actuators. The $St_F = 0.03$ case shows an increase of the boundary layer velocity over most of the measurement plane while the $St_F = 0.5$ case is less successful and appears more similar to the baseline flow.

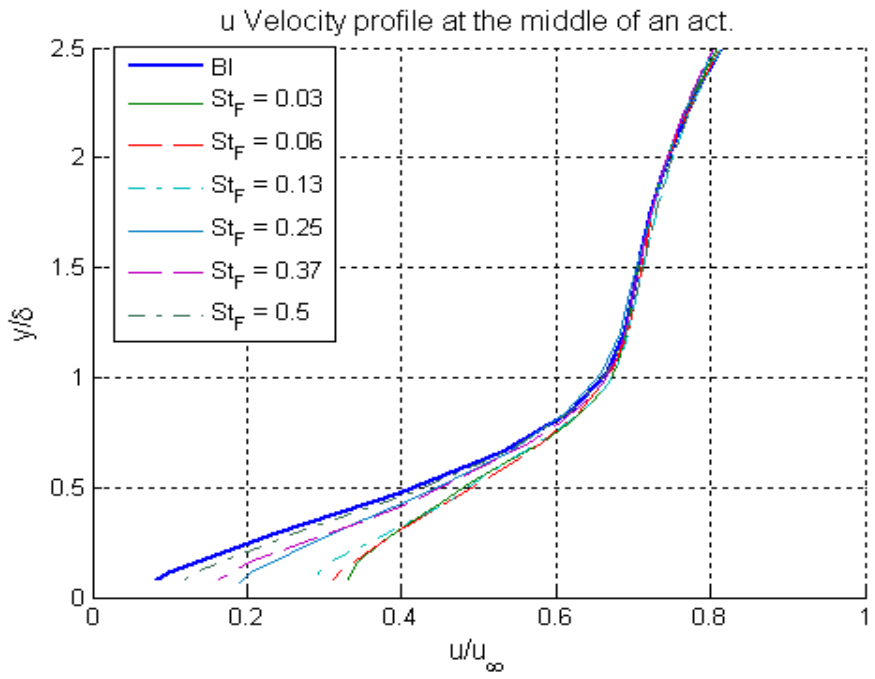

Figure 11: Effect of the LAFPAs on the Interaction Region ($X^* = -0.29$ and $X_a^* = -1.25$)

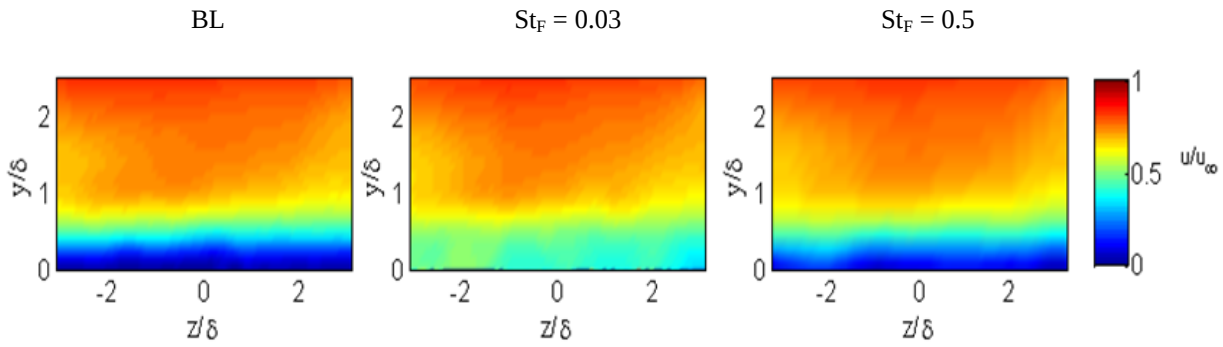

Figure 12: Velocity Maps of Baseline and Forced Cases (X* = -0.29 and Xa* = -1.25)

Stereoscopic PIV measurements further downstream at $X^* = 0.38$ (not shown) exhibit no noticeable plasma actuation effect on the flow field. This is somewhat expected from the Schlieren image shown in Figure 9 where the expansion fan, generated at the trailing edge of the shock generator, has reached the flow near the floor of the test section for the measurement plane at $X^* = 0.38$. We suspect that the expansion fan, which nearly restores the flow to pre-shock conditions, is interfering or possibly hiding the effect of actuation in this region. To eliminate the interference of the expansion fan, we have designed a new and larger facility in order to allow more distance over which to analyze the flow downstream of the

SWBLI before it encounters the expansion wave. Another possibility is that the effects of forcing decay through the impinging shock.

Figure 13 compares the baseline flow with the flow with forcing in-phase, and every other actuator operating 180° out of phase for $St_F = 0.06$ with the actuators at $X_a^* = -1.25$. The test was performed to determine how the increased three-dimensionality of the forcing would affect the control ability of the actuators. The velocity maps are acquired at $X^* = -0.29$. It can be seen that forcing out-of-phase has little effect on the flow since the velocity map is almost identical to the baseline. The reason that the actuators have almost no effect in the out-of-phase case is not yet understood and will require a more detailed investigation. Further examination of the number and relative phase of the actuators will be pursued in the future.

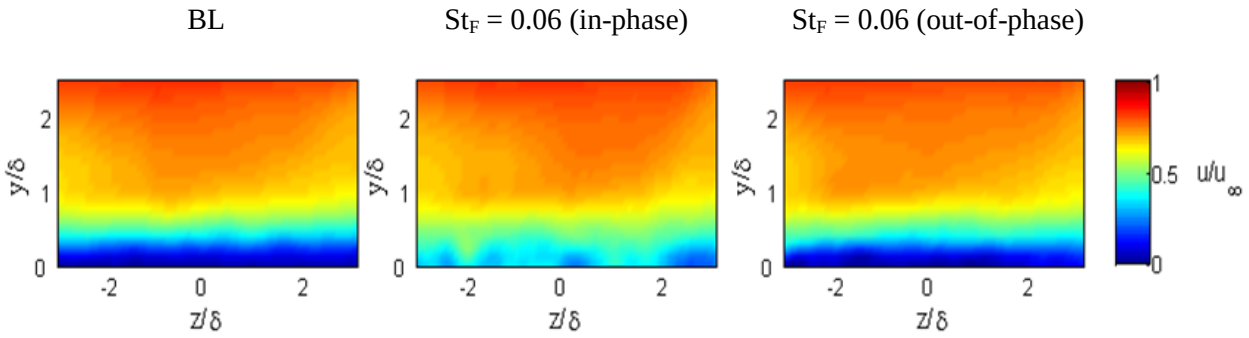

Figure 13: Comparison of the Effects of In-Phase and Out-of-Phase Forcing

Figure 14 shows the streamwise velocity profiles for various forcing Strouhal numbers when the actuators are located at $X_a^* = -0.83$ and operated in-phase. Again, the profiles shown are on the centerline of an actuator and represent the typical behavior of the flow at different spanwise locations. In this setup, the actuators are located within the SWBLI region slightly downstream of the reflected shock. The actuators create significantly less change in the velocity profile than in the previous case (Figure 11).

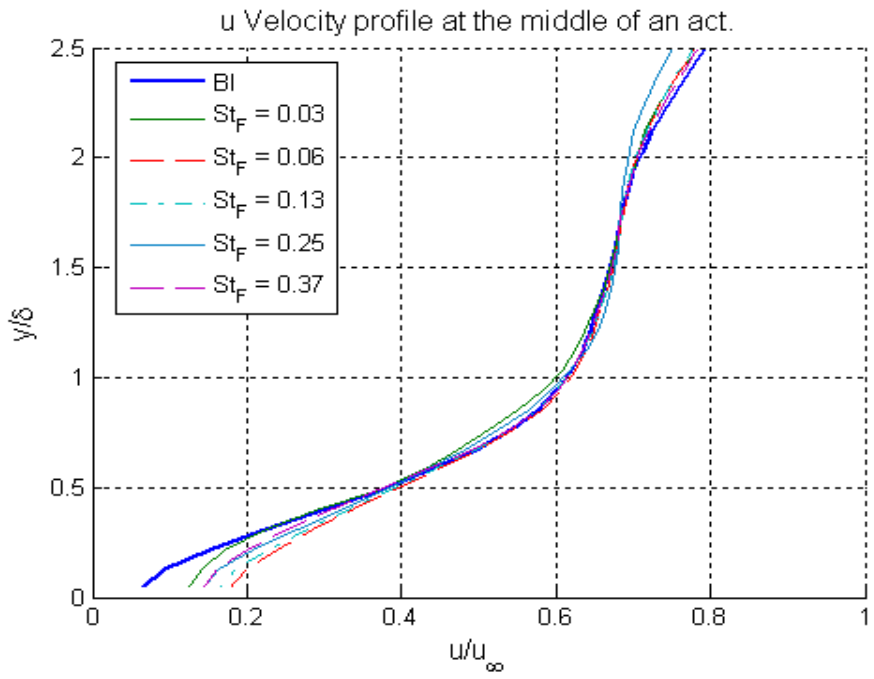

Figure 14: Effect of the LAFPAs when Located Within the Interaction (X* = -0.29 and Xa* = -0.83)

Figure 15 shows the u-velocity maps for two of the cases shown in Figure 14. Again little change in the flow can be observed when forcing is introduced within the interaction region. This may provide some insight into the control mechanism involved. The potential mechanism is associated with manipulation of the unsteady characteristics of the SWBLI using the unsteady forcing capabilities of LAFPAs. It was observed that the forcing may be manipulating the unsteady nature of the reflected shock. Therefore, it is intuitive that the technique would be more effective if the actuation takes place upstream of the interaction region. Based on this argument the actuators would not be expected to be effective when located within the separated region. This is in agreement with the current results. Future work is intended to examine these issues further.

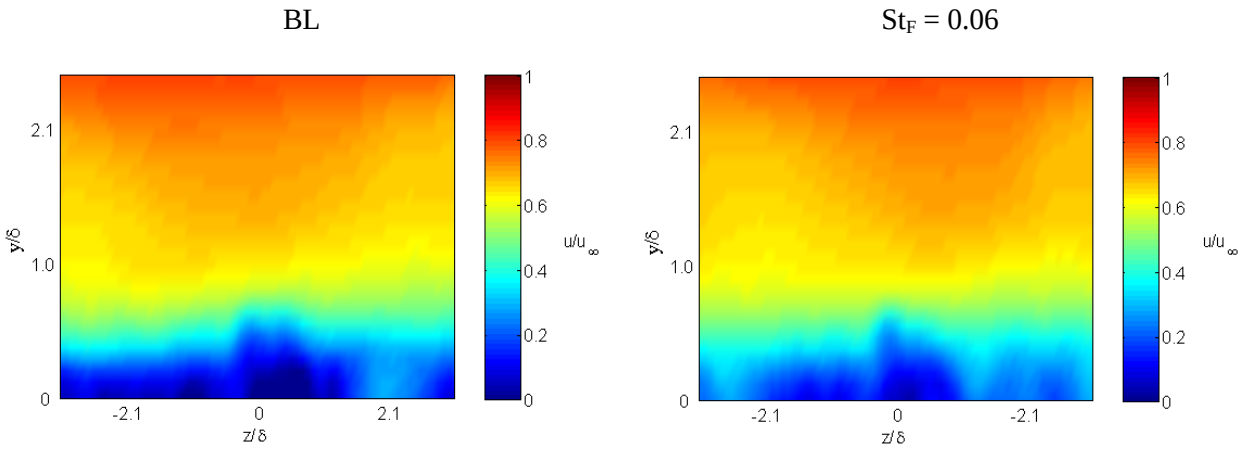

Figure 15: Velocity Maps of the LAFPA's Effects when Located Within the Interaction ($X^* = -0.29$, $X_a^* = -0.83$)

3.2 Variable Angle Wedge Results

3.2.1 Measurements of Baseline Flow Field

3.2.1.1 Schlieren Imaging

The first diagnostic used to examine the baseline flow is schlieren imaging. This is used mainly as a qualitative technique that takes little time to set up, run, and process to verify that the flow is clean, and free of strong extraneous shocks/expansions. Additionally, schlieren images provide qualitative and quantitative information regarding the nature and extent of the SWBLI. The presence of all of the documented features of the interaction, primary/reflected shocks, separated region, and expansion over the separated region, are verified. Additionally, the schlieren image is scaled to allow the interaction length to be measured from the image. This length is used to normalize the frequencies associated with the interaction. Schlieren images for each of the three measured deflection angles/interaction strengths are shown in Figure 16a-c. It should be noted that these images are not instantaneous, they are time-averaged by the shutter speed of the camera, and by ensemble averaging 15 images. These images show good agreement with Figure 1 in regards to the general structure of the interaction. It should also be noted (Figure 16a and b) that the wedge seems to be generating two primary shock waves. This is deceptive and is the result of the integrating effect of the schlieren technique over the collimated optical path. The "secondary shock" that is observed is believed to be the curving or bowing of the shock around the spanwise edge of the partial span shock generator.

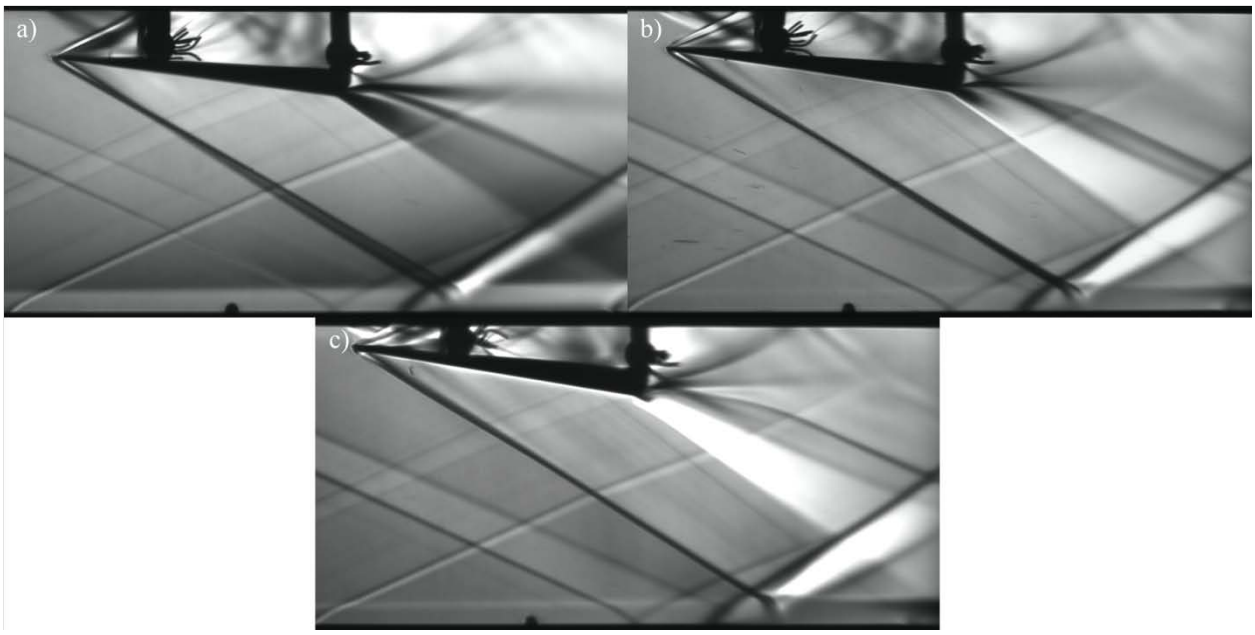

Figure 16: Schlieren Images of the SWBLI; a) 7°, b) 8°, c) 9°.

3.2.1.2 PIV Measurements

Streamwise two-component PIV measurements are used to determine general operating parameters such as the freestream velocity and boundary layer properties. Figure 17 is a streamwise velocity map on a streamwise-vertical plane. It is an ensemble average of 200 vector fields, which is sufficient for statistically converged mean flow. This figure also shows good agreement with Figure 1 regarding the general structure of a SWBLI. Unfortunately, due the small height of the separation region, the difficulty of making PIV measurements in close proximity to a wall, and the PIV measurements spatial resolution, no reversed flow is actually observed.

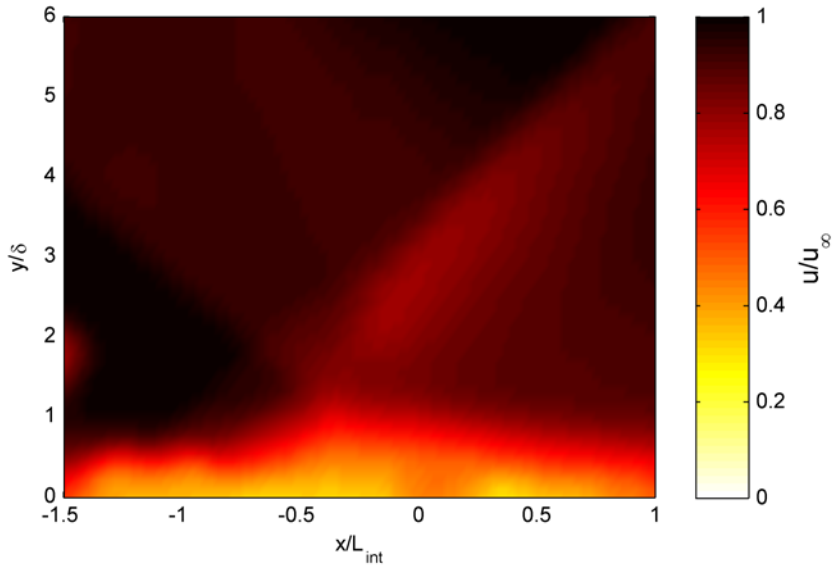

Figure 17: Streamwise Velocity Map of the SWBLI for the Baseline Flow.

The upstream boundary layer profile and van Driest transformed profile are shown in Figure 18 at a location of X^* = -1.15. Although the flow was intuitively known to be turbulent, due to the large distance of ~35 cm from the last characteristics line within the nozzle to the measurement location over which it is allowed to naturally develop, more concrete evidence is desired. Thus the van Driest transformed profile was compared to the turbulent model profile proposed by Maise and McDonald.[28] The van Driest transformation is given by

$$\frac{u_\infty^* - u^*}{u_\tau} = -\frac{1}{\kappa}\ln\left(\frac{y}{\delta}\right) + \frac{\Pi}{\kappa}\left(1 + \cos\frac{\pi y}{\delta}\right) \tag{1}$$

where $\kappa = 0.4$ is the Karmen mixing length constant, Π is the wake strength parameter, and u_τ is the friction velocity. The normalized velocity, u^*, is given by

$$u^* = \frac{u_\infty}{A}\sin^{-1}\left[\frac{2A^2(u/u_\infty) - B}{(B^2 + 4A^2)^{1/2}}\right] \tag{2}$$

where

$$A^2 = \frac{[(\gamma - 1)/2]\, M_\infty^2}{T_w/T_\infty} \tag{3}$$

$$B = \frac{1 + [(\gamma - 1)/2]\, M_\infty^2}{T_w/T_\infty} - 1 \tag{4}$$

and T_w/T_∞ is the ratio between wall and freestream temperatures. The Maise and McDonald model profile is given by κ = 0.4 and Π = 0.5.[28] The good agreement observed confirms that the incoming boundary layer is fully developed and turbulent.

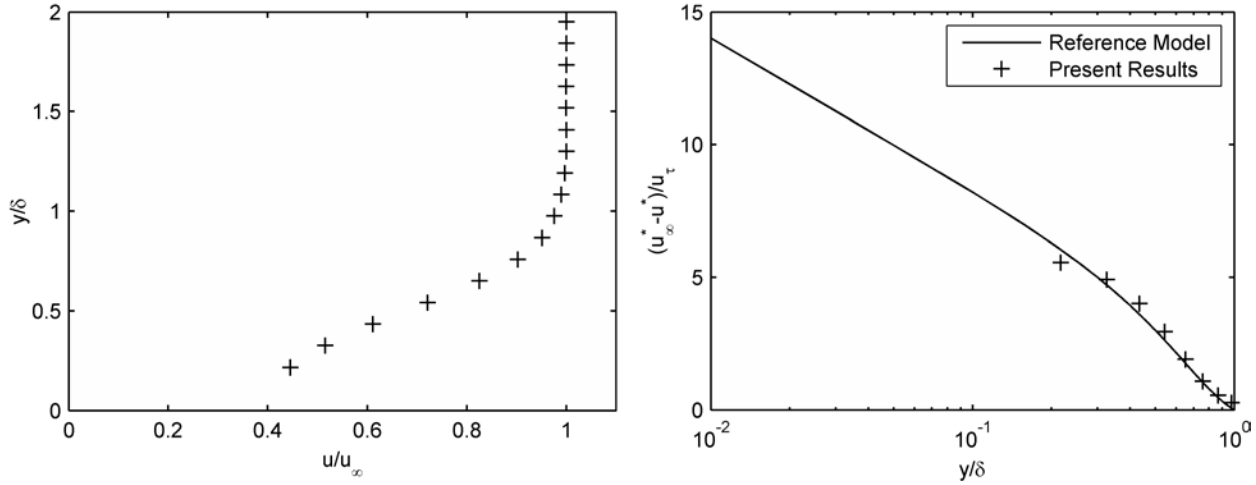

Figure 18: a) Upstream Velocity Profile (*X = -1.15) and b) van Driest Transformed Profile Compared with Maise and McDonald[28] Turbulent Model.**

The upstream boundary layer properties are calculated from the profile shown in Figure 18. The results of these calculations are displayed in Table 1. The integral quantities (δ^* and θ) are calculated using both standard incompressible equations as well as accounting for compressibility using the method described in Schlicting[29]. The integrals for the latter are expressed as

$$\delta_c^* = \int_0^\delta 1 - \frac{u}{1 + r[(\gamma - 1)/2]M_\infty^2[1 - (u/u_\infty)^2]}\, dy \tag{5}$$

and

$$\theta_c = \int_0^\delta \frac{u(1 - u)}{1 + r[(\gamma - 1)/2]M_\infty^2[1 - (u/u_\infty)^2]}\, dy \tag{6}$$

where u is a function of y, and r is taken to be 0.896. The calculated incompressible values match well with the reported values in the literature. The shape factor (H) taken at $X^* = -1.15$ is slightly higher than most of those found in the literature, but this simply means the boundary layer is more susceptible to separation.

Table 1: Freestream and Boundary Layer Flow Properties.

Type	X^*	δ [mm]	δ^* [mm]	θ [mm]	H	Re_θ
Compressible	-1.15	5.35	2.28	0.53	4.27	24,800
Incompressible	-1.15	5.35	1.40	0.78	1.79	36,200

After the PIV data were analyzed, the flow was determined to be clean and a desirable environment in which to test the control authority of the LAFPAs. Additional measurement techniques are then used to investigate further the baseline flow before exploring the effects of the LAFPAs on the SWBLI.

3.2.1.3 Surface Oil Flow Visualization

Surface oil flow visualizations are conducted to provide information concerning the three-dimensionality of the flow field. Figure 19a-c shows de-skewed images of the surface oil flow images taken while the tunnel was operating. The images are taken from the side window while the tunnel was running and therefore have to be de-skewed. A few observations can be made from these images. Firstly, the flow is highly three-dimensional over the span of the tunnel, but a central region, approximately 60% of the tunnel width, is relatively two-dimensional in nature. This 2-D region is a canonical representation of a SWBLI. However, recent research has shown that even the 2-D region, specifically the severity of the separation, is affected by the overall three-dimensionality of the interaction.[30] Secondly, separation is clearly visible in all three of the interaction strengths. Thirdly, the most noticeable change between the three cases is the two-dimensionality of the 2-D region. While the extent of the 2-D region remains relatively constant throughout the various interaction strengths, the two-dimensionality increases with increasing shock strength. At first glance, this seems counterintuitive: intuition would lead to the conclusion that the sidewall interactions would be strengthened by the increasing shock strength, thus leading to a more highly three-dimensional centerline interaction. However, the strengthening of the shock seems to increase the two-dimensionality of the interaction by making the centerline separation stronger. This is believed to be a consequence of the partial span of the wedge. A full span wedge with the same cross-sectional profile has since been made and has been shown to exhibit the expected behavior: increasing three-dimensionality due to corner flows with increasing wedge angle.

The reattachment line is difficult to observe in the still images. It can be more easily observed in movies taken while the facility is operating. The pertinent information, such as shock foot location, separation line, reattachment line, and 2-D region are marked in each of the figures. Although not much is currently known regarding the effects of the sidewalls on the centerline interaction, they have been shown

to be present. It is therefore good practice to assess qualitatively the magnitude of the sidewall interactions to more completely characterize the flow.

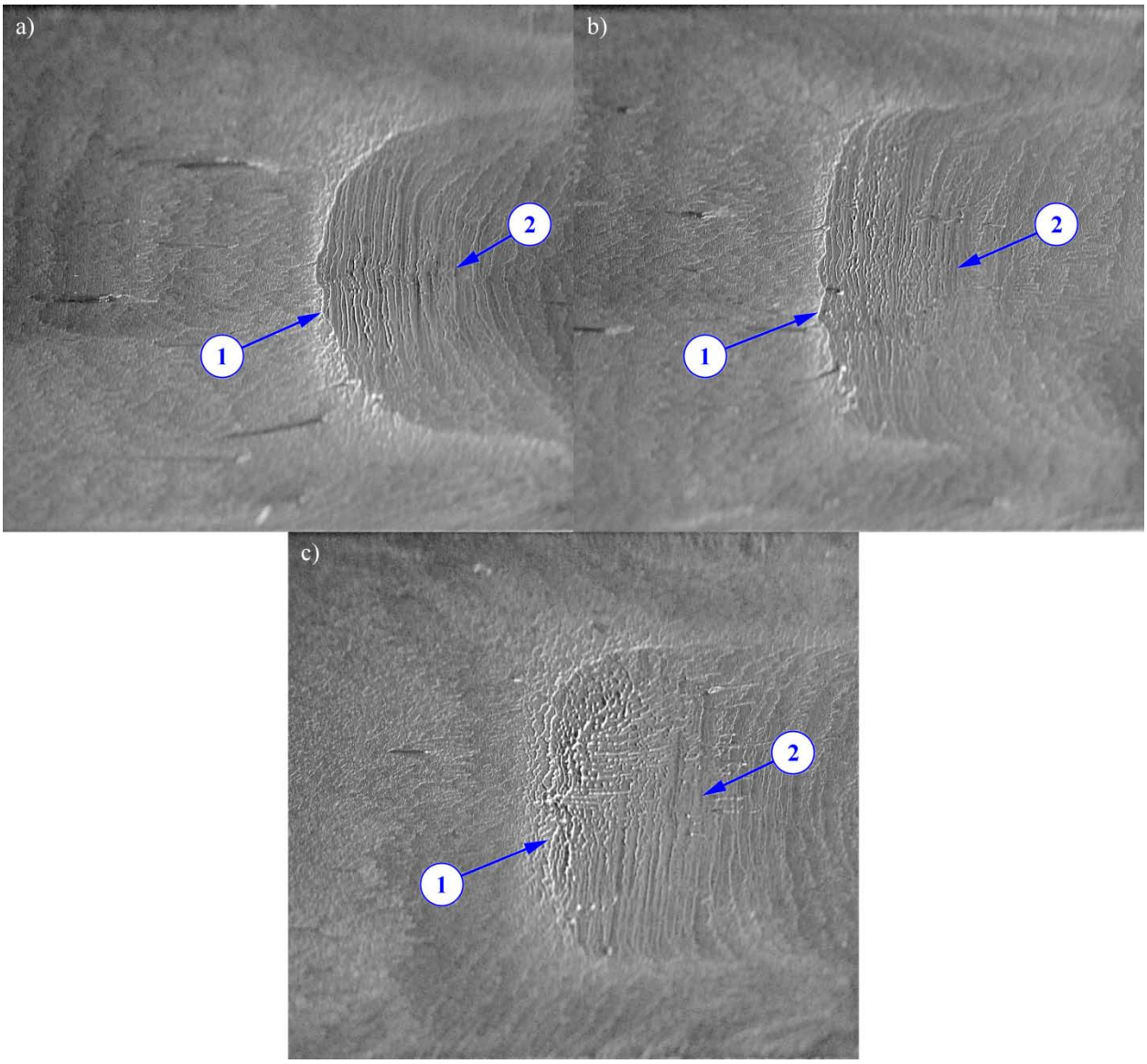

Figure 19: Surface Oil Flow Images of Various Interaction Strengths in Baseline Flow Showing (1) Separation and (2) Reattachment Lines; a) 7°, b) 8°, c) 9°.

3.2.1.4 Time-Resolved Pressure Measurements

The unsteady nature of the interaction is a characteristic of great interest due to its significant effects in applications and the current ongoing research regarding the physical sources of it. In particular, as previously mentioned, there is significant research currently being conducted to determine the mechanism by which the low frequency oscillations of the reflected shock foot are generated. The fundamental

physics of the interaction is important to active flow control that utilizes instabilities of the flow. The large scale of the natural oscillations in the flow suggests that if the fundamental mechanism can be taken advantage of using an active control technique, a significant effect on the flow could be generated. In order to investigate the unsteadiness of the interaction, time-resolved pressure measurements are taken beneath the interaction using Kulite pressure transducers. Figure 8 shows the location of the transducers. Figures 20 and 21 show the normalized-weighted and weighted power spectral density, respectively, of the pressure signals for the three different wedge angles. The weighted PSD, given in Equation 7 accentuates amplitude of the pressure fluctuations, while the normalized-weighted PSD, given in Equation 8, accentuates frequency content of the pressure fluctuations.

$$PSD_{wt}(f) = PSD(f) \cdot f \tag{7}$$

$$PSD_{n.wt}(f) = \frac{PSD_{wt}(f)}{\int_0^\infty PSD_{wt}(\xi)\, d\xi} \tag{8}$$

Previous research has shown two dominant frequency components in the interaction region: a low Strouhal number, largely 2-D oscillation with a broad peak centered at $St \approx 0.03$ and a higher Strouhal number oscillation with a broad peak centered at $St \approx 0.5$.[2,8] The broad low Strouhal number peak is clearly noted upstream of the reflected shock foot. The results shown in Figure 20 confirm these findings and clearly show the dominance of the low Strouhal number oscillation in the upstream and the high Strouhal number oscillations in further downstream. The pressure data also show the same shift in peak frequency from the low to high in the interaction region as observed by Dupont et al.[8] It has been proposed previously that the breathing motion of the separation region, as it entrains mass and subsequently sheds structures, is responsible for this oscillation.[13] The scalability of the frequencies of this interaction is yet another piece of evidence that this method of normalizing the interaction frequency components is correct.

Note that the data in Figure 21 was intentionally not normalized and plotted on a logarithmic ordinate to allow comparison of the absolute amplitude of the observed fluctuations. Comparison of the results in Figure 21 a), b) and c) reveal that the relative dominance of the low frequency components increases and moves downstream as the interaction strength increases. This trend is also found in the literature.[14]

The frequencies discovered within the interaction provided a starting point for the forcing experiments. By providing information regarding the natural instabilities within the interaction, they suggest instabilities that might be exploited in order to control the flow. Section III.B. discusses the results of the forcing experiments.

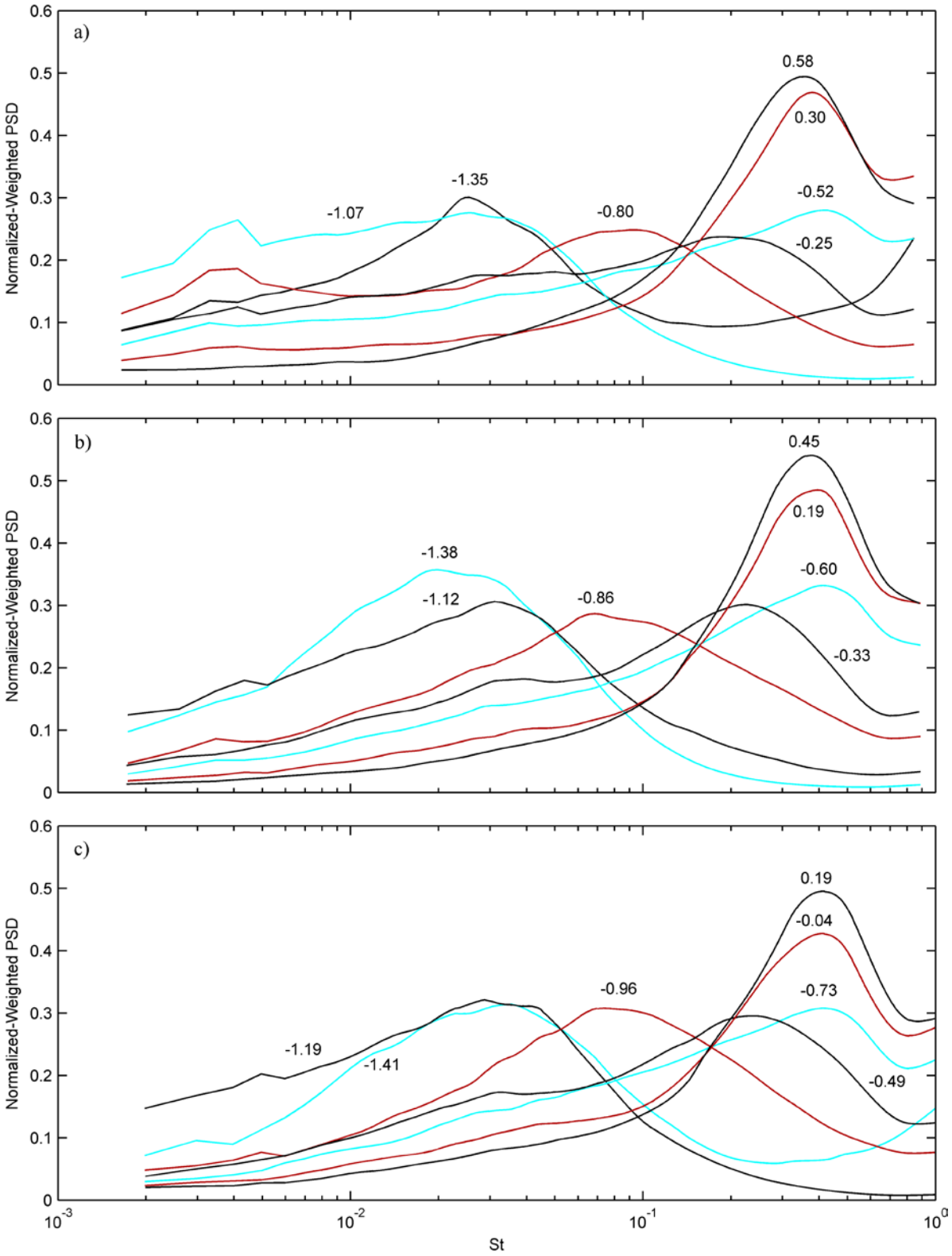

Figure 20: Normalized-Weighted Power Spectral Density on the Centerline of the Test Section within the Interaction Region; a) 7°, b) 8°, c) 9°.

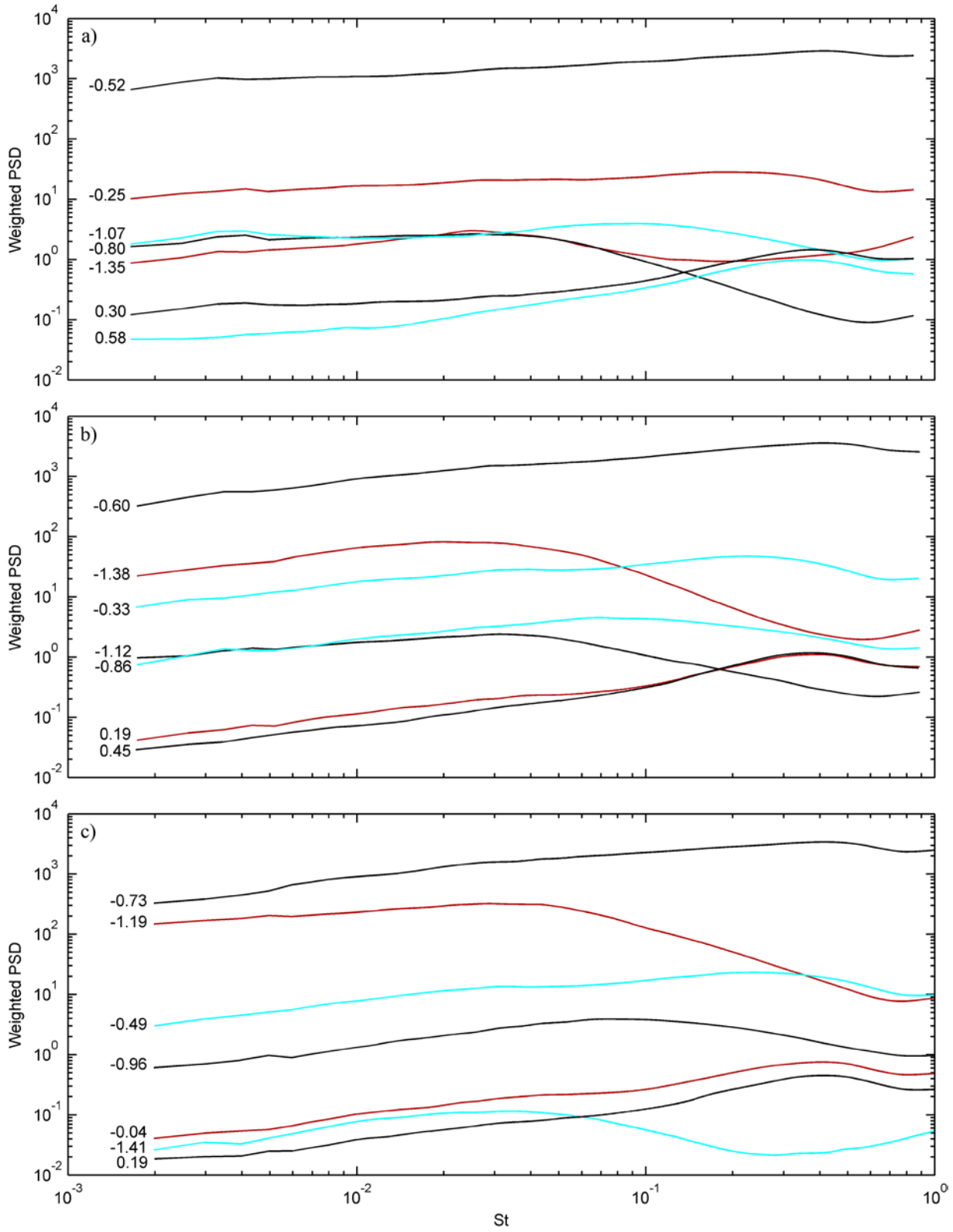

Figure 21: Weighted Power Spectral Density on the Centerline of the Test Section within the Interaction Region; a) 7°, b) 8°, c) 9°.

3.3 Results of Forced Cases

Our previous preliminary results using LAFPAs to control SWBLI had been carried out in a Mach 1.9 flow with a 10° ramp.[31] Figure 11 taken from the compression ramp work shows normalized velocity profiles in one location within the interaction region ($X^* = -0.29$) for the optimum actuator location. The trend is quite clear and shows that the flow responds to forcing and the boundary layer is significantly energized when the actuators operated at $St \approx 0.03$ and the flow response drops as the forcing Strouhal number is moved away from this Strouhal number. In both facilities, eight actuators were uniformly distributed on a single line in the spanwise direction, as shown in Figure 5, and all the actuators were operated at the same time (the same phase). However, the flow response disappeared when the adjacent actuators were operated 180° out-of-phase. This is consistent with the theoretical finding of Touber and Sandham[32] that the instability associated with this low Strouhal number oscillation is nominally two-dimensional.

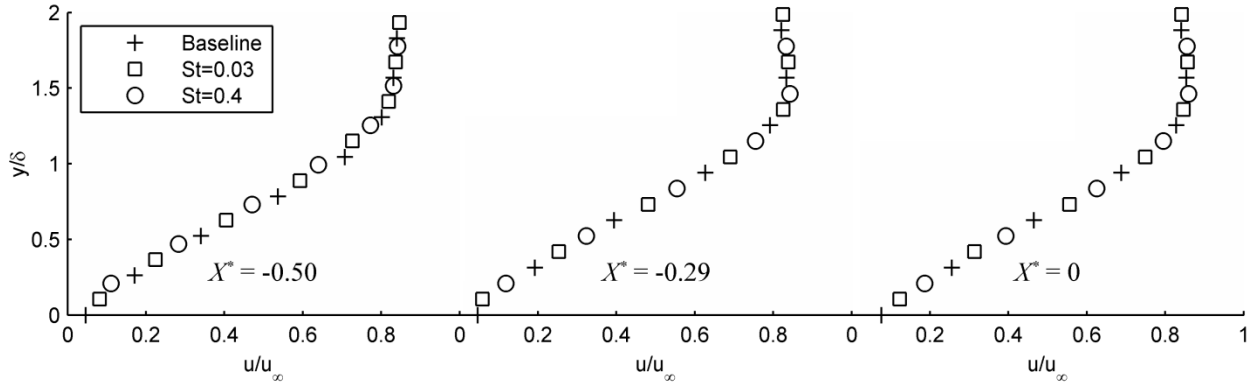

Figure 22: Velocity Profiles at Three Locations within the Interaction for the Baseline and Two Forcing Cases with Strouhal Numbers of 0.03 and 0.4.

As was discussed earlier, the variable angle wedge facility is designed using a wedge (Figure 16) rather than a ramp with two main reasons in mind. The first one is to eliminate any unsteadiness associated with the primary impinging shock wave itself. The second one is to make the wedge angle variable enabling investigation of SWBLI of different strength and the response of the SWBLI with different strength to actuation. It is well known that any flow instability has a receptivity range with an optimal location. While the two objectives were met, there was no means of optimizing the actuator location for a given ramp angle. We have recently added such a capability and are in the process of locating an optimal receptivity region. Figure 22 shows normalized velocity profiles in three locations within the interaction region for forcing Strouhal numbers of 0.03 and 0.4. The actuation does not seem to have any effect with this actuator location.

4 Summary

The purpose of the preliminary study was to determine whether localized arc filament plasma actuators (LAFPAs) are capable of controlling shock wave boundary layer interactions in a supersonic mixed compression type inlet. It was also intended to establish some of the important parameters such as forcing Strouhal number, phase difference between actuators and actuator location that would maximize the effectiveness of the actuators. In order to fulfill these objectives a supersonic wind tunnel facility was modified to accommodate the SWBLI test section. The baseline flow was characterized using schlieren imaging and stereoscopic PIV. The flow was forced using a spanwise array of eight LAFPAs, which were operated with varying forcing Strouhal number, phase difference between adjacent actuators, and actuator position. The preliminary results showed that near the wall, the normalized streamwise velocity increased from 0.08 to 0.35 when the flow was forced at $St_F = 0.03$ with all actuators operating in-phase and the actuators located at $X_a^* = -1.25$, just slightly upstream of the SWBLI location. The relative phase difference between actuators was also examined. When every other actuator operated out-of-phase the actuation showed significantly less effect on the flow than when all the actuators operated in-phase. Results for the actuators placed just inside the SWBLI region showed that the control is significantly less effective in comparison to when they are located upstream.

The results indicate that the LAFPAs exert control authority over a SWBLI by manipulating natural instabilities within the interaction. Forcing seems to manipulate the unsteady nature of the reflected shock since the effect is more significant when forcing close to the characteristic Strouhal number of the leading edge of the interaction as measured by Dupont et al.[25]. The effectiveness of control decreases as the Strouhal number of the forcing is increased. Intuitively this control mechanism would seem to place the maximum receptivity region (the region in which the SWBLI is receptive to controlling perturbations) upstream of the reflected shock. The preliminary work would support this conclusion as placing the LAFPAs downstream of the reflected shock was found to significantly decrease their effectiveness.

In order to expand upon the preliminary compression ramp experiments, a new and larger test section was designed and built to enable ease of interrogation of the interaction and surrounding region. Additionally a variable-angle wedge shock generator was employed to quickly and easily test a wide variety of SWBLI strengths.

As a first step, the baseline flow was characterized using schlieren imaging and PIV measurements. The results were compared with existing SWBLI descriptions in the literature, as well as checked to ensure that the flow was clean and was without extraneous shocks. Additionally the incoming boundary layer was closely examined and compared to normalized, compressible, turbulent boundary layer profiles in literature. This confirmed that the incoming boundary layer was fully turbulent.

Recently other work has shown that the three-dimensional nature of the interaction plays a role in the dynamics that govern even the quasi-two-dimensional region at the tunnel centerline. Surface oil flow visualization was used to examine the three-dimensionality of the interaction. The interaction was found to be more two-dimensional as the strength was increased. This unexpected trend seems to stem from the partial span wedge. A full span wedge has since shown the expected trend of increasing three-dimensionality as shock strength is increased.

Time-resolved pressure measurements are used to investigate the unsteady nature of the interaction region, and to guide the selection of forcing frequencies. The flow unsteadiness is shown to match well with the results found in the current literature.

The facility was unable to impose sufficient control authority of the LAFPAs due to the inability to modify the streamwise location of the actuators with sufficient resolution. This is an important capability in any active control based on excitation of instabilities due to the possibility of a potentially small receptivity region. Therefore, the facility has been modified to allow the location of the LAFPAs to be adjusted. The debugging of the system is currently underway. After the system has been debugged, experiments will be conducted to attempt to replicate the findings of the compression ramp facility in the new tunnel. The research into the LAFPAs control authority, the mechanism, the effect of operating parameters, and optimization of the control authority will be continued.

5 References

[1]Dolling, D. S., "Fifty Years of Shock-Wave/Boundary-Layer Interaction Research: What Next?," *AIAA Journal*, Vol. 39, No. 8, 2001, pp. 1517-1531.

[2]Touber, E. and Sandham, N. D., "Large-Eddy Simulation of Low-Frequency Unsteadiness in a Turbulent Shock-Induced Separation Bubble," *Theoretical and Computational Fluid Dynamics*, Vol. 23, 2009, pp. 79-107.

[3]Syberg, J. and Koncsek, J. L., "Experimental Evaluation of an Analytically Derived Bleed System for a Supersonic Inlet," *Journal of Aircraft*, Vol. 13, No. 10, 1976, pp. 792-797.

[4]Anderson, B. H., Tinapple, J. and Surber, L., "Optimal Control of Shock Wave Turbulent Boundary Layer Interactions Using Micro-Array Actuation," 3rd Flow Control Conference 2006-3197, 2006.

[5]Babinsky, H., Li, Y. and Ford, C. P., "Microramp Control of Supersonic Oblique Shock-Wave/Boundary-Layer Interactions," *AIAA Journal*, Vol. 47, No. 3, 2009, pp. 668-675.

[6]Ogawa, H. and Babinsky, H., "Shock/Boundary-Layer Interaction Control Using Three-dimensional Bumps in Supersonic Engine Inlets," 46th Aerospace Sciences Meeting and Exhibit 2008-599, 2008.

[7]Gefroh, D., Loth, E., Dutton, C. and McIlwain, S., "Control of an Oblique Shock/Boundary-Layer Interaction with Aeroelastic Mesoflaps," *AIAA Journal*, Vol. 40, No. 12, 2002, pp. 2456-66.

[8]Dupont, P., Haddad, C. and Debiève, J. F., "Space and Time Organization in a Shock-Induced Separated Boundary Layer," *Journal of Fluid Mechanics*, Vol. 559, 2006, pp. 255-277.

[9]Plotkin, K. J., "Shock Wave Oscillation Driven by Turbulent Boundary Layer Fluctuations," *AIAA Journal*, Vol. 13, No. 8, 1975, pp. 1036-40.

[10]Beresh, S. J., Clemens, N. T. and Dolling, D. S., "Relationship Between Upstream Turbulent Boundary-Layer Velocity Fluctuations and Separation Shock Unsteadiness," *AIAA Journal*, Vol. 40, No. 12, 2002, pp. 2412-2422.

[11]Ganapathisubramani, B., Clemens, N. and Dolling, D., "Low-frequency Dynamics of Shock-Induced Separation in a Compression Ramp Interaction," *Journal of Fluid Mechanics*, Vol. 636, 2009, pp. 397-425.

[12]Humble, R., Elsinga, G., Scarano, F. and Oudheusden, B. v., "Three-Dimensional Instantaneous Structure of a Shock Wave/Turbulent Boundary Layer Interaction," *Journal of Fluid Mechanics*, Vol. 622, 2009, pp. 33-62.

[13]Piponniau, S., Dussauge, J., Debieve, J. and Dupont, P., "A Simple Model for Low-Frequency Unsteadiness in Shock-Induced Separation," *Journal of Fluid Mechanics*, Vol. 629, 2009, pp. 87-108.

[14]Agostini, L., Larchevêque, L., Dupont, P., Debiève, J.-F. and Dussauge, J.-P., "Zones of Influence and Shock Motion in a Shock Boundary Layer Interaction," 49th AIAA Aerospace Sciences Meeting 2011-728, 2011.

[15]Pirozzoli, S. and Grasso, F., "Direct numerical simulation of impinging shock wave/turbulent boundary layer interaction at M=2.25," *Physics of Fluids A*, Vol. 18, 2006, pp. 1-17.

[16]Kalra, C. S., Zaidi, S. and Miles, R. B., "Shockwave Induced Turbulent Boundary Layer Separation Control with Plasma Actuators," 48th Aerospace Sciences Meeting and Exhibit 2008-1092, 2008.

[17]Narayanaswamy, V., Raja, L. L. and Clemens, N. T., "Characterization of a High-Frequency Pulsed-Plasma Jet Actuator for Supersonic Flow Control," *AIAA Journal*, Vol. 48, No. 2, 2010, pp. 297-305.

[18]Leonov, S. B., Firsov, A. A., Yarantsev, D. A., Falempin, F. and Miller, A., "Flow Control in Model Supersonic Inlet by Electrical Discharge," AIAA 16th International Space Planes and Hypersonic Systems and Technologies Conference 2009-7367, 2009.

[19]Samimy, M., Kim, J.-H., Kastner, J., Adamovich, I. and Utkin, Y., "Active Control of a Mach 0.9 Jet for Noise Mitigation Using Plasma Actuators," *AIAA Journal*, Vol. 45, No. 4, 2007, pp. 890-901.

[20]Samimy, M., Kim, J.-H., Kastner, J., Adamovich, I. and Utkin, Y., "Active Control of High-Speed and High-Reynolds-Number Jets Using Plasma Actuators," *Journal of Fluid Mechanics*, Vol. 578, No. 1, 2007, pp. 305-330.

[21]Utkin, Y. G., Keshav, S., Kim, J.-H., Kastner, J., Adamovich, I. V. and Samimy, M., "Development and Use of Localized Arc Filament Plasma Actuators for High-Speed Flow Control," *Journal of Physics D: Applied Physics*, Vol. 40, No. 3, 2007, pp. 685-694.

[22]Kalra, C. S., Zaidi, S. H., Miles, R. B. and Macheret, S. O., "Shockwave-Turbulent Boundary Layer Interaction Control Using Magnetically Driven Surface Discharges," *Experiments in Fluids*, Vol. 50, 2011, pp. 547-559.

[23]Hahn, C., Kearney-Fischer, M. and Samimy, M., "Effects of Ring Groove and Duty Cycle on Plasma Actuator Performance in High Speed Jets," 49th AIAA Aerospace Sciences Meeting 2011-977, 2011.

[24]Berthe, A., Kondermann, D., Christensen, C., Goubergrits, L., Garbe, C., Affeld, K. and Kertzscher, U., "Three-Dimensional, Three-Component Wall-PIV," *Experiments in Fluids*, Vol. 48, 2010, pp. 983-997.

[25]Dupont, P., Haddad, C. and Debieve, J. F., "Space and Time Organization in a Shock-Induced Separated Boundary Layer," *Journal of Fluid Mechanics*, Vol. 559, No. 1, 2006, pp. 255-277.

[26]Samimy, M., Zaman, K. B. M. Q. and Reeder, M. F., "Effect of Tabs on the Flow and Noise Field of an Axisymmetric Jet," *AIAA Journal*, Vol. 31, No. 1, 1993, pp. 609-619.

[27]Kim, J.-H. and Samimy, M., "Mixing Enhancement via Nozzle Trailing Edge Modifications in a High Speed Rectangular Jet," *Physics of Fluids*, Vol. 11, No. 9, 1999, pp. 2731-2742.

[28]Maise, G. and McDonald, H., "Mixing Length and Kinematic Eddy Viscosity in a Compressible Boundary Layer," *AIAA Journal*, Vol. 6, No. 1, 1968, pp. 73-80.

[29]Schlicting, H."Boundary-Layer Theory,"editted by Kestin, J.

[30]Burton, D., Babinsky, H. and Bruce, P., "Experimental Investigations into Parameters Governing Corner Interaction for Transonic Shock Wave/Boundary Layer Interactions," AIAA 48th Aerospace Sciences Meeting 2010-0871, 2010.

[31]Caraballo, E., Webb, N., Little, J., Kim, J.-H. and Samimy, M., "Supersonic Inlet Flow Control Using Plasma Actuators," 47th AIAA Aerospace Sciences Meeting 2009-924, 2009.

[32]Williamson, C., Weierman, J. and Jacob, J., "Flow Control in an Axial Compressor using Plasma Actuators," AIAA Paper 2009-4290, 2009.